Coherent oscillations of electrons in tunnel-coupled wells under ultrafast intersubband excitation

2004 J. Phys.: Condens. Matter 16 5327

(http://iopscience.iop.org/0953-8984/16/29/022)

INSTITUTE OF PHYSICS PUBLISHING JOURNAL OF PHYSICS: CONDENSED MATTER

J. Phys.: Condens. Matter **16** (2004) 5327–5338 PII: S0953-8984(04)77591-8

Coherent oscillations of electrons in tunnel-coupled wells under ultrafast intersubband excitation

A Hernández-Cabrera[1], **P Aceituno**[1] **and F T Vasko**[2]

[1] Departamento de Física Básica, Universidad de La Laguna, La Laguna 38206-Tenerife, Canary Islands, Spain
[2] Institute of Semiconductor Physics, NAS of Ukraine, Kiev, 252650, Ukraine

E-mail: ajhernan@ull.es

Received 9 March 2004
Published 9 July 2004
Online at stacks.iop.org/JPhysCM/16/5327
doi:10.1088/0953-8984/16/29/022

Abstract

Ultrafast intersubband excitation of electrons in tunnel-coupled wells is studied in respect of its dependence on the structure parameters, the duration of the infrared pump and the detuning frequency. The temporal dependences of the photoinduced carrier concentration and dipole moment are obtained for two cases of transitions: from the single ground state to the tunnel-coupled excited states and from the tunnel-coupled states to the single excited state. The peculiarities of dephasing and population relaxation processes are also taken into account. The nonlinear regime of the response is also considered when the splitting energy between the tunnel-coupled levels is renormalized by the photoexcited electron concentration. The dependences of the period and the amplitude of oscillations on the excitation pulse are presented with a description of the damping of the nonlinear oscillations.

1. Introduction

The coherent dynamics of electrons in heterostructures has been thoroughly examined during the past decade for the case of the interband ultrafast excitation by a near-infrared (IR) pulse (see [1] for review). Recently, a mid-IR pump has also been employed for the treatment of the coherent dynamics of electrons under the intersubband excitation; see the review [2] and in [3, 4]. Although the intersubband transitions in heterostructures are similar to the multi-level model widely used in the optics of atomic systems [5], a special consideration is necessary for tunnel-coupled heterostructures. For example, a coherent transfer of electrons between tunnel-uncoupled states of a double quantum well (DQW) to the common excited state under a mid-IR pump was considered in [6]. Moreover, a new type of semiconductor unipolar laser operating in the mid-infrared spectral region has been demonstrated. This type of device is based on a three-bound-state coupled DQW with a single-excited level and two coupled lower levels [7].

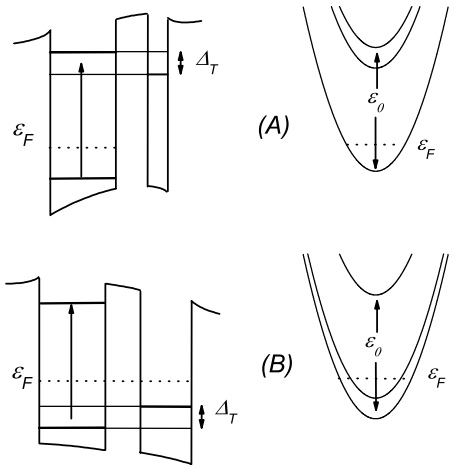

Figure 1. Band diagrams and dispersion laws for the intersubband excitation of tunnel-coupled wells with single-ground (A) or single-excited (B) states.

To the best of our knowledge, an investigation of the coherent dynamics in tunnel-coupled DQWs under ultrafast mid-IR pump has not yet been performed. The key question here is the possibility to observe these oscillations under an effective intersubband scattering. In the present work we carry out the theory of the ultrafast response on the intersubband excitation between the tunnel-coupled states and the single level, which can be ground or excited, and we demonstrate the possibility for observation of the ultrafast response under a mid-IR pump.

The study we will fulfill next is based on the quantum kinetic equation for the density matrix averaged over the pump frequency, excluding the intersubband polarization at the mid-IR frequency (see evaluation in [8, 9]). We will discuss the effects of the intersubband transition peculiarities by means of the intersubband generation rate, taking into account the coherent superposition of the tunnel-coupled states. With this purpose we take into account the peculiarities of the intersubband excitation for two cases: (A) when the electron transition occurs between the single-ground and the tunnel-coupled excited states, or (B) when the transition takes place from the tunnel-coupled states to the single-excited state. To illustrate these scenarios we have represented in figure 1 the band diagrams and the dispersion laws for two DQW samples of GaAs/$Al_{0.35}Ga_{0.65}$As/GaAs, with layer widths of 150/130/40 Å and 150/20/120 Å, corresponding to the cases (A) and (B), respectively. We have chosen the DQW structures in such a way that the energy separation between the coupled sublevels, Δ_T, is about 10 meV and the mid-IR pump energy is about 50 meV for both cases. In this context the population relaxation is controlled by the LO phonon emission [10], while the dephasing of the tunnel-coupled states for case (B) is determined by the quasi-elastic scattering; we describe these relaxation processes by introducing the corresponding relaxation times. Thus, for the case of the second-order response we have obtained an explicit description of the response. Since the interwell redistribution of the charge appears under a relatively low pump intensity, we have also considered the nonlinear regime of oscillations, solving the system of nonlinear equations for the population of the single level and the 2×2 density matrix of the tunnel-coupled states. Moreover, we will compare the present results with the corresponding ones for the interband excitation case.

The paper is organized as follows. In section 2 we derive the balance equations, which describe the coherent response of electrons in DQWs under the ultrafast

intersubband excitation. In section 3 we discuss the emerging quantum beats and the peculiarities of the coherent response under the finite duration excitation, stressing the differences between the cases of intersubband and interband excitation. Section 4 contains the description of the nonlinear response. The conclusions and discussion of the approximations used are given in the last section.

2. Balance equations

The coherent dynamics of the electrons, when photoexcited by an ultra-short pulse, is described below in the framework of the second-order response on the intersubband excitation. Performing the average over the period of the radiation we obtain the quantum kinetic equation for the density matrix, $\hat{\rho}_t$, in the following form (see [8, 9]):

$$\frac{\partial \hat{\rho}_t}{\partial t} + \frac{\mathrm{i}}{\hbar}[\hat{H}, \hat{\rho}_t] = \hat{G}_t + \hat{I}_{sc}, \tag{1}$$

where $\hat{H}$ is the Hamiltonian of the DQWs under consideration, $\hat{I}_{sc}$ is the collision integral, and $\hat{G}_t$ is the intersubband generation rate. When the electrons are excited by a transverse electric field $E_\perp w_t \exp(-\mathrm{i}\omega t) + \text{c.c.}$, with a frequency ω and an envelope function w_t, the generation rate is given by

$$\hat{G}_t = \frac{1}{\hbar^2}\int_{-\infty}^{0} \mathrm{d}\tau\, \mathrm{e}^{\lambda\tau - \mathrm{i}\omega\tau}\left[\mathrm{e}^{\mathrm{i}\hat{H}\tau/\hbar}\left[\widehat{\delta h}_{t+\tau}, \hat{\rho}_{\mathrm{eq}}\right]\mathrm{e}^{\mathrm{i}\hat{H}\tau/\hbar}, \widehat{\delta h}_t^{+}\right] + \text{h.c.} \tag{2}$$

Here $\lambda \to 0$, the perturbation operator, $\widehat{\delta h}_t = (\mathrm{i}e/\omega)E_\perp \hat{v}_\perp w_t$, is written through the transverse velocity operator $\hat{v}_\perp$ and $\hat{\rho}_{\mathrm{eq}}$ is the equilibrium density matrix when the second-order contributions to the response are taken into account.

Neglecting the non-resonant mixing between the single and the tunnel-coupled levels, we describe the system by the scalar distribution function, $F_{\mathbf{p}t}^{(k)}$, where $k = 0, ex$ correspond to the single electron state (ground $|0\rangle$ or excited $|ex\rangle$ state for the cases (A) or (B), respectively), and by the 2×2 matrix function $\hat{f}_{\mathbf{p}t}$ which describes the tunnel-coupled states $|u\rangle$ and $|l\rangle$ (upper and lower, respectively). Within the framework of the momentum representation, with the in-plane momentum $\mathbf{p}$, equation (1) is transformed into

$$\begin{aligned} &\frac{\partial F_{\mathbf{p}t}^{(k)}}{\partial t} = G_{\mathbf{p}t}^{(k)} + I_{sc}^{(k)}(F_t|\mathbf{p}), \\ &\frac{\partial \hat{f}_{\mathbf{p}t}}{\partial t} + \frac{\mathrm{i}}{\hbar}[\hat{h}_{\mathrm{DQW}}, \hat{f}_{\mathbf{p}t}] = \hat{G}_{\mathbf{p}t} + \hat{I}_{sc}(\hat{f}_t|\mathbf{p}), \end{aligned} \tag{3}$$

where $\hat{h}_{\mathrm{DQW}} = (\Delta/2)\hat{\sigma}_z + T\hat{\sigma}_x$ is the matrix Hamiltonian of the tunnel-coupled states, Δ is the interlevel splitting energy, T is the tunnel matrix element, and $\hat{\sigma}_{x,z}$ are the Pauli matrices. Here the generation rates are different for the cases (A) and (B). Neglecting the overlap between $|k\rangle$ and $|l\rangle$ states, when $\langle 0|\hat{v}_\perp|l\rangle \simeq 0$, and doing the straightforward calculations of equation (2), we obtain for the case (A)

$$\begin{aligned} \begin{vmatrix} G_{\mathbf{p}t}^{(0)} \\ \langle j\mathbf{p}|\hat{G}_t|\mathbf{p}j'\rangle \end{vmatrix} &= \theta(\varepsilon_{\mathrm{F}} - \varepsilon_{\mathrm{p}})\left(\frac{eE_\perp}{\hbar\omega}\right)^2 |\langle 0|\hat{v}_\perp|u\rangle|^2 w_t \int_{-\infty}^{0} \mathrm{d}\tau\, w_{t+\tau}\mathrm{e}^{\tau/\tau_2 - \mathrm{i}\Delta\omega\tau} \\ &\times \begin{vmatrix} -\langle u|\exp(\mathrm{i}\hat{h}_{\mathrm{DQW}}\tau/\hbar)|u\rangle \\ \langle j|\exp(\mathrm{i}\hat{h}_{\mathrm{DQW}}\tau/\hbar)|j\rangle\delta_{uj'} \end{vmatrix} + \text{h.c.}, \end{aligned} \tag{4}$$

where $\theta(\varepsilon_{\mathrm{F}} - \varepsilon_{\mathrm{p}})$ is the ground state equilibrium distribution for the zero temperature case, ε_{F} is the Fermi energy, and $\varepsilon_{\mathrm{p}} = p^2/2m$ is the kinetic energy with the effective mass m. The dephasing time, τ_2, is introduced here instead of the λ-parameter of equation (2) with the aim

of describing a finite broadening of the intersubband transitions. For the case (B) we use $\langle ex|\hat{v}_\perp|l\rangle \simeq 0$, and the generation rate takes the form

$$\left| \begin{array}{c} G^{(ex)}_{\mathbf{p}t} \\ \langle j\mathbf{p}|\hat{G}_t|\mathbf{p}j'\rangle \end{array} \right| = \left(\frac{eE_\perp}{\hbar\omega}\right)^2 |\langle ex|\hat{v}_\perp|u\rangle|^2 w_t \int_{-\infty}^{0} \mathrm{d}\tau\, w_{t+\tau} \mathrm{e}^{\tau/\tau_2 - \mathrm{i}\Delta\omega\tau} \times \left| \begin{array}{c} -\langle u|\hat{\rho}_{\mathrm{DQW}} \exp(-\mathrm{i}\hat{h}_{\mathrm{DQW}}\tau/\hbar)|u\rangle \\ \delta_{ju}\langle u|\hat{\rho}_{\mathrm{DQW}} \exp(-\mathrm{i}\hat{h}_{\mathrm{DQW}}\tau/\hbar)|j'\rangle \end{array} \right| + \mathrm{h.c.}, \tag{5}$$

where $\hat{\rho}_{\mathrm{DQW}}$ is the equilibrium density matrix of the tunnel-coupled levels. The detuning frequency in equations (4), (5), $\Delta\omega = \omega - \varepsilon_{\mathrm{o}}/\hbar$, is evaluated through the energy difference between single and tunnel-coupled levels, ε_{o} (see figure 1). The remaining matrix elements in equations (4), (5) are calculated by using the matrix equalities:

$$\begin{aligned} &\exp(-\mathrm{i}\hat{h}_{\mathrm{DQW}}\tau/\hbar) = \cos\Omega_T\tau/2 + \mathrm{i}\frac{\Delta\hat{\sigma}_z + 2T\hat{\sigma}_x}{\Delta_T}\sin\Omega_T\tau/2, \\ &\hat{\rho}_{\mathrm{DQW}} = f_\varepsilon^{(+)} + \frac{\Delta\hat{\sigma}_z + 2T\hat{\sigma}_x}{\Delta_T} f_\varepsilon^{(-)}. \end{aligned} \tag{6}$$

Here $\Omega_T = \Delta_T/\hbar$ is the frequency of oscillations due to transitions between tunnel-coupled levels, $\Delta_T = \sqrt{\Delta^2 + (2T)^2}$ and $f_\varepsilon^{(\pm)} = [\theta(\varepsilon_F - \varepsilon - \Delta/2) \pm \theta(\varepsilon_F - \varepsilon + \Delta/2)]/2$.

When doing the summation over the 2D momenta we introduce the population of the single level, $N_t = (2/L^2)\sum_{\mathbf{p}} F_{\mathbf{p}t}$, and the 2×2 matrix of concentration $(2/L^2)\sum_{\mathbf{p}} \hat{f}_{\mathbf{p}t} = n_t + (\mathbf{n}_t \cdot \hat{\boldsymbol{\sigma}}_t)$, which is written through the scalar and vector components of the concentration, n_t and $\mathbf{n}_t$. Due to the particle conservation law, $N_t + n_t = n_{2\mathrm{D}}$ with the total 2D concentration $n_{2\mathrm{D}}$, the system (3) is transformed into the balance equations

$$\frac{\mathrm{d}n_t}{\mathrm{d}t} = -\frac{\mathrm{d}N_t}{\mathrm{d}t} = G(t) - S(t), \qquad \frac{\mathrm{d}\mathbf{n}_t}{\mathrm{d}t} - [\mathbf{L} \times \mathbf{n}_t] + \boldsymbol{\Sigma}(t) = \mathbf{G}(t), \tag{7}$$

where $S(t) = n_t^u/\tau_1$ for the case (A) or $S(t) = n_t/\tau_1$ for the case (B) and $n_t^u = n_t + n_t^z$. The vector $\boldsymbol{\Sigma}(t)$ is defined as $\boldsymbol{\Sigma}(t) = (0, 0, n_t^u/\tau_1)$ (case (A)) or $\boldsymbol{\Sigma}(t) = \hat{\nu}\mathbf{n}_t$ (case (B)). Here τ_1 stands for the population relaxation time between single level and tunnel-coupled states, while the vector $\mathbf{L} = (2T/\hbar, 0, \Delta/\hbar)$ describes the dynamic properties of the tunnel-coupled electronic states. The relaxation matrix in the case (B), $\hat{\nu}$, is determined by the non-zero components $(\hat{\nu})_{xx} = (\hat{\nu})_{yy} = \tau_0^{-1}$, where the dephasing relaxation time, τ_0, was introduced in [11] for the case of elastic scattering in DQWs. The generation rates $G(t)$ and $\mathbf{G}(t) = [G_x(t), G_y(t), G(t)]$ are obtained from equations (4) to (6) in the form

$$\begin{bmatrix} G_x(t) \\ G_y(t) \end{bmatrix} = \frac{2T}{\Delta_T}\frac{\mathcal{N}w_t}{\pi}\int_{-\infty}^{0}\frac{\mathrm{d}\tau}{\tau_{\mathrm{p}}^2} w_{t+\tau}\mathrm{e}^{\tau/\tau_2} \times \left\{ a_+ \begin{bmatrix} -\cos(\Delta\omega + \Omega_T/2)\tau \\ \sin(\Delta\omega + \Omega_T/2)\tau \end{bmatrix} - a_- \begin{bmatrix} -\cos(\Delta\omega - \Omega_T/2)\tau \\ \sin(\Delta\omega - \Omega_T/2)\tau \end{bmatrix} \right\}, \tag{8}$$

$$G(t) = \frac{\mathcal{N}w_t}{\pi}\int_{-\infty}^{0}\frac{\mathrm{d}\tau}{\tau_{\mathrm{p}}^2} w_{t+\tau}\mathrm{e}^{\tau/\tau_2}\left[b_+\cos(\Delta\omega + \Omega_T/2)\tau + b_-\cos(\Delta\omega - \Omega_T/2)\tau\right]. \tag{9}$$

The characteristic photoinduced concentration in equations (8), (9) is determined as

$$\mathcal{N} = \frac{\pi n_{2\mathrm{D}}}{2}\left(\frac{eE_\perp v_\perp}{\hbar\omega}\tau_{\mathrm{p}}\right)^2 \tag{10}$$

with the characteristic pulse duration τ_{p}. The intersubband velocities $v_\perp^2$ are equal to $|\langle 0|\hat{v}_\perp|l\rangle|^2$ or $|\langle ex|\hat{v}_\perp|l\rangle|^2$ for the cases (A) or (B), respectively, and $v_\perp$ definition is given in [11]. The coefficients $a_\pm$ in equation (8) are given by $a_\pm = (1 \pm \Delta n/n_{2\mathrm{D}})/2$ (moreover,

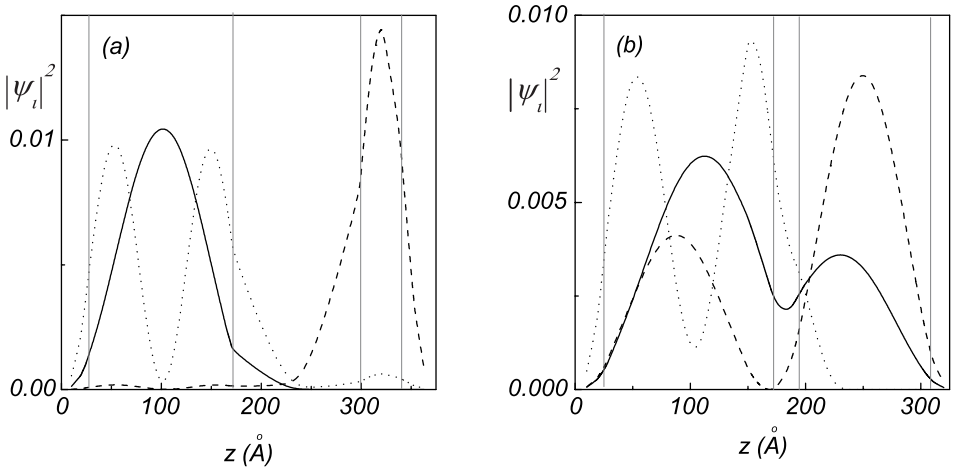

Figure 2. Square of the wavefunctions close to the resonance. (*a*) Structure (A). Solid curve: single-ground level. Dashed curve: lower coupled-level. Dotted curve: upper coupled level. (*b*) Structure (B). Solid curve: lower coupled-level. Dashed curve: upper coupled-level. Dotted curve: single-excited level. Vertical lines indicate the position of the DQW interfaces.

$\Delta n = 0$ for DQW (A)) while, in equation (9), $b_\pm = 1 \mp \Delta/\Delta_T$ for the case (A) and $b_\pm = (1 \pm \Delta/\Delta_T)(1 \pm \Delta n/n_{2D})/2$ for DQW (B), where $\Delta n = \rho_{2D}\Delta_T$.

Next, taking into account the Coulomb renormalization of the tunnel-coupled levels, we have to replace $\hat{h}_{DQW}$ in the matrix equation (3) by the Hartree–Fock Hamiltonian, $\tilde{h}_{DQW}$, written in the form[3] (see [12, 13])

$$\tilde{h}_{DQW} = \hat{h}_{DQW} + \sum_{\mathbf{Q}} v_Q \left[n_{\mathbf{Q}t} e^{-i\mathbf{Q}\cdot\mathbf{r}} - e^{-i\mathbf{Q}\cdot\mathbf{r}} \hat{\rho}_t e^{i\mathbf{Q}\cdot\mathbf{r}} \right]. \tag{11}$$

Here $\mathbf{Q}$ is the 3D wavevector, v_Q is the Coulomb matrix element, and $n_{\mathbf{Q}t} = \mathrm{Tr}(\hat{\rho}_t e^{i\mathbf{Q}\cdot\mathbf{r}})$ is the Fourier transform of the electron density. Further transformations lead to the balance equation (7) with the renormalized vector $\mathbf{L}_t$ written through the level splitting energy

$$\Delta(t) = \Delta \pm \frac{4\pi e^2}{\epsilon} Z(n_t^z - n_t), \tag{12}$$

where Z is the distance between the centres of l- and r-QWs and ϵ is the dielectric permittivity supposed to be uniform across the DQWs. The signs + and − in equation (12) correspond to the cases (A) and (B), respectively. The evaluation of $\Delta(t)$ coincides with that done for DQW (A) in [12].

In order to obtain numerical results for energy levels and, therefore, for Δ and T, we have self-consistently solved the coupled Schrödinger and Poisson equations for both DQWs [14]. Figures 2(*a*), (*b*) show the square of the wavefunctions for structures (A) and (B), respectively, corresponding to a situation close to the coupled-level resonance. Due to the large size of the central barrier chosen for the first structure, the coupling between the two excited states is weak, as reflected in figure 2(*a*). In contrast, the resonant levels of structure (B) are strongly coupled. As was commented on before, the sizes have been chosen so that the interband and intersubband energy values are roughly the same for both structures. Under resonant conditions, the

[3] Note that the same τ_1 appears in the population balance equation and here because we neglect the overlap between $|0\rangle$ and $|l\rangle$ states.

transverse velocities are $|\hat{v}_\perp| \sim 9 \times 10^5$ cm s^{-1} for DQW (A), and $|\hat{v}_\perp| \sim 1 \times 10^6$ cm s^{-1} for DQW (B).

It should be stressed that the key role is played by the z-component of the vector concentration n_t^z, which is proportional to the dipole moment and, thus, a directly measurable physical magnitude, together with the excited carrier concentration n_t.

3. Quantum beats

In this section we present a solution of the linear system of balance equations (7), neglecting the second addendum in equation (12), for the cases of short and finite pulse duration. With respect to the short-pulse approximation, if the pulse duration $\tau_p \ll |\Delta\omega|^{-1}, \Omega_T^{-1}$, the generation rates (equations (8) and (9)) take the forms $G_x(t) \simeq -a_+(2T/\Delta_T)\mathcal{N}\delta_p(t)$, $G_y(t) \simeq 0$, and $G(t) \simeq b_+\mathcal{N}\delta_p(t)$, with the δ-like function $\delta_p(t) = (2w_t/\pi)\int_{-\infty}^{0} d\tau\, w_{t+\tau}/\tau_p^2$. Thus, the photoinduced redistribution of the carrier concentration can be written as the step-like function $n_t = b_+\mathcal{N}\int_{-\infty}^{t} dt'\,\delta_p(t')$, which is proportional to the step function $\theta(t)$ if $\tau_p \to 0$. Since the photoinduced dipole moment is expressed through n_t^z, we obtain the z-component of $\mathbf{n}_t$ in the form

$$n_t^z = \theta(t)\mathcal{N}\left\{\cos\left[\frac{\Omega_T}{2}(t-\tau_p)\right] + \cos(\Omega_T t)\right\}. \tag{13}$$

For the short-pulse approximation, the differences between the above-presented results and those corresponding to the case of the interband excitation (as considered in [8]) are mainly attributable to the different characteristic concentrations and to the strong damping caused by the interband relaxation. Comparing equation (10) with the characteristic carrier concentration for the interband excitation, N^* (given by the equation (18) in [8]), we obtain

$$\frac{\mathcal{N}}{N^*} \simeq \frac{4n_{2D}\tau_p}{\rho_{2D}^*\hbar}\left(\frac{E_\perp}{E^*}\frac{v_\perp\varepsilon_g}{\mathcal{P}\varepsilon_o}\right)^2, \tag{14}$$

where the interband excitation is characterized by the Kane velocity $\mathcal{P}$, the gap ε_g, the reduced density of states ρ_{2D}^*, and the field strength E^*. If $E_\perp \sim E^*$, and the pulse is not too short ($\tau_p \sim 1$ ps), the ratio (14) is about 16 (case (A)) and 26 (case (B)) for the GaAlAs-based structures with a total 2D-concentration $n_{2D} \simeq 1.4 \times 10^{11}$ cm^{-2} and the dimensions used in figure 1. Thus, the intersubband excitation appears to be more effective than the interband one.

The response seems to be more complicated for the finite pulse duration case due to the peculiarities of the relaxation processes. We have used below the Gaussian envelope function, $w_t = \exp[-(t/\tau_p)^2/2]$, a semiempirical value of the damping $\tau_0 = 35$ ps [15], a dephasing time caused by the finite broadening of the intersubband transition $\tau_2 = 1$ ps [16, 17] and an interband relaxation time due to LO phonons $\tau_1 = 3.5$ ps [7, 17]. We consider first the evolution of the carrier concentration. Figure 3 shows the evolution of n_t with the increase of the pulse duration $\tau_p\Omega_T/2\pi$, for three detuning frequencies $\Delta\omega = 0$, $\Delta\omega = \Omega_T/2$, and $\Delta\omega = \Omega_T$ (figures 3(a)–(c), respectively) and for DQW (A). Due to the different character of the involved transitions, the photoexcited carrier concentration n_t in DQW (B) shows a different behaviour from that corresponding to the structure (A). Panel 2(d) represents the concentration profile for DQW (B) when $\Delta\omega = 0$ and for five different pulse duration times. A new non-monotonic behaviour appears in all these cases in contrast to that of the interband excitation case [8]. For $0 \lesssim \tau_p\Omega_T/2\pi < 1$, $n_t/\mathcal{N}$ behaves like in the interband case (corresponding to the short pulse context) with some types of oscillation superimposed. For $\tau_p\Omega_T/2\pi \gtrsim 1$, $n_t/\mathcal{N}$ these oscillations are strongly amplified around $t = 0$ for $\Delta\omega = 0$ and $\Delta\omega = \Omega_T$, when the excited sublevel(s) is (are) not tuned, before decaying. It should be noted that the

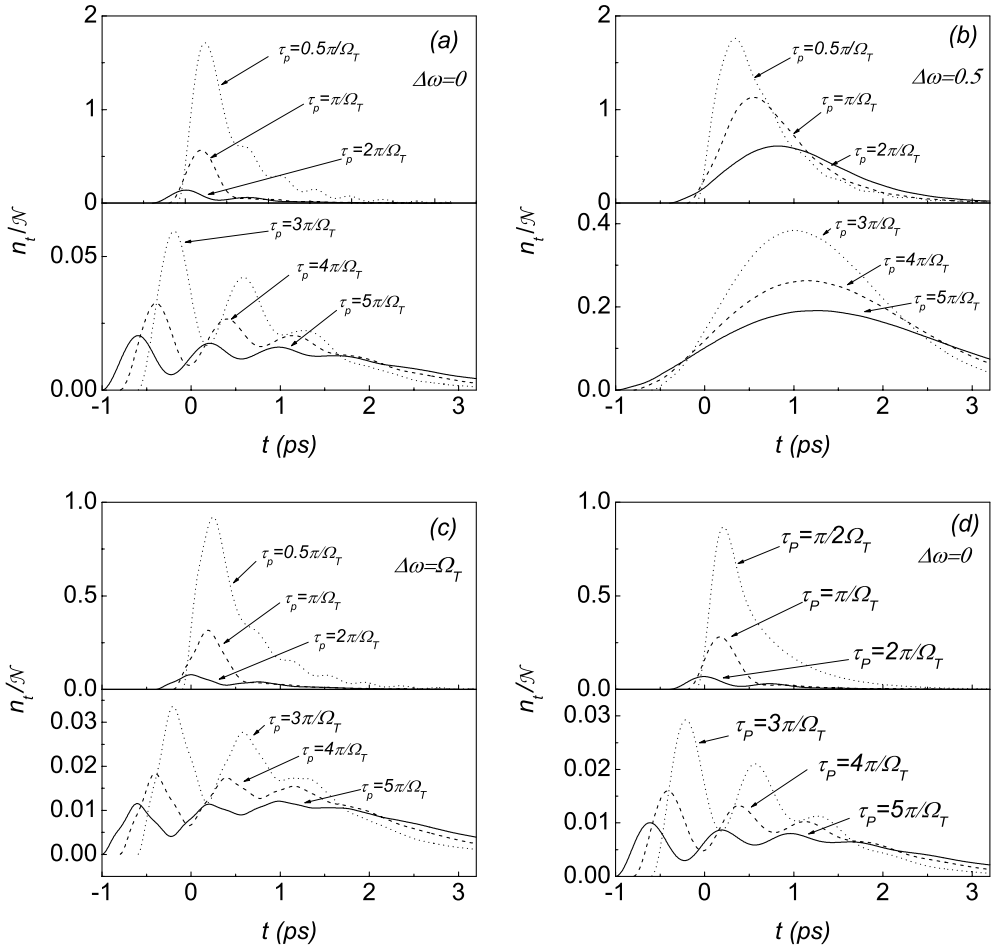

Figure 3. Temporal evolution profile of the excited electron concentration n_t for different pulse duration values. Panels ((*a*)–(*c*)) correspond to the structure (A) for different detuning frequencies. Panel (*d*) corresponds to the structure (B). Pulse duration times are indicated by arrows with $\pi/\Omega_T = 0.44$ ps.

excitation pulse is centred at $t = 0$. The number of oscillations depends on the pulse duration $\tau_{\rm p}$, as figures 3(*a*), (*c*) display. It is important to note that these oscillations have a period $2\pi/\Omega_T$, twice the n_t^z quantum beats period, because such oscillations are controlled by the term $\Delta\omega + \Omega_T/2$ and strongly influence the initial stages of n_t^z. An exception takes place when one of the levels is tuned, e.g., $\Delta\omega = \pm\Omega_T/2$. Then, the carrier concentration shows a monotonic behaviour with a growth rate similar to that of the interband pump (figure 3 (b)). Also visible in figure 3 is the exponential damping of the photoexcited electrons caused by the dephasing time, τ_2.

Figures 4 and 5 illustrate the temporal evolution of the dipole moment, which is proportional to n_t^z, for different regions of parameters, $\tau_{\rm p}$, $\eta = \Delta/\Delta_T$, and $\Delta\omega$. Figures 4(*a*), 5(*a*) are for sample (A) and figures 4(*b*), 5(*b*) for sample (B), respectively. The main difference between the finite pulse excitation and the short pulse excitation is the existence of two different regimes in the former event. This peculiarity seems to be more evident in the structure (B). When $\Delta\omega = 0$ and $\eta = 0$ (upper panels of figures 4(*a*), (*b*))

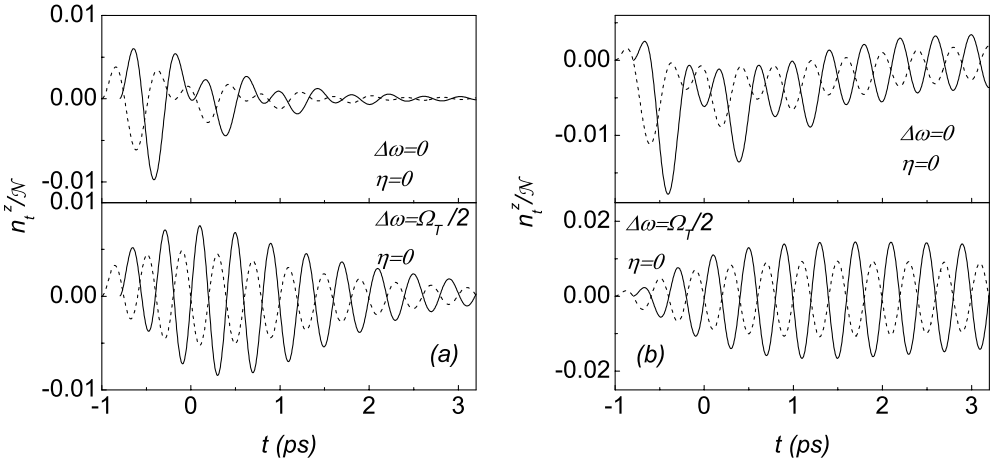

Figure 4. Temporal evolution of $n_t^z/\mathcal{N}$ for $\eta = 0$. Figures 4(a) and (b) correspond to structures (A) and (B), respectively. Solid and dashed curves are plotted for $\tau_p = 1.76$ ps (zero-phase shift) and for $\tau_p = 2.2$ ps (π-phase shift). The upper and lower panels correspond to $\Delta\omega = 0$ and $\Omega_T/2$.

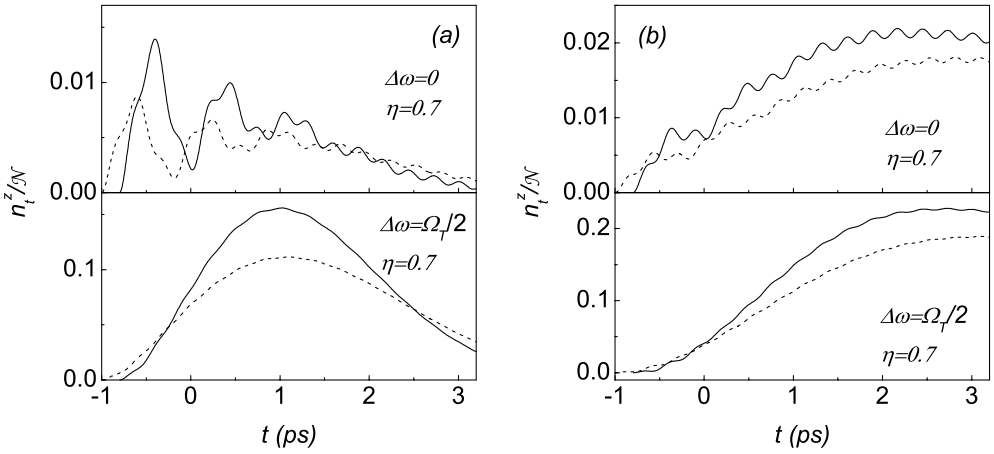

Figure 5. The same as in figure 4 for $\eta = 0.7$. Solid curve: $\tau_p = 1.76$ ps.

the finite pulse produces a transition from a regime in which the electron density is mainly located in a well to two-well oscillations. This transition occurs when the pulse is switched off. The dipole moment exhibits a bigger oscillation amplitude while the pulse holds and Rabi oscillations are dominant. After switching off the pulse, the quantum beats become dominant and the oscillations decay due to relaxation until they reach equilibrium when the photoexcited carrier concentration is equally distributed between the wells. The balance situation is different for the two samples studied. In case (A) the electronic redistribution between both wells is quickly reached because the photoexcited electrons decay from the coupled levels to the ground state by means of the LO phonon emission. We must keep in mind that we are representing here the distribution n_t^z corresponding to the coupled excited levels. In contrast, in the second sample, (B), we are representing the carrier concentration for the non-excited coupled levels. In this case the electronic balance redistribution between the wells is caused by the intersubband

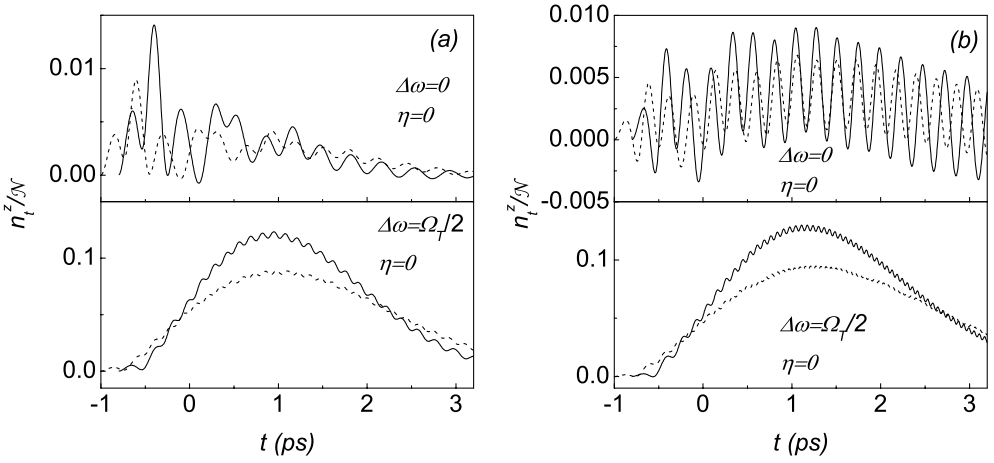

Figure 6. Nonlinear regime of the dipole moment $n_t^z/\mathcal{N}$ for $\eta = 0$. Figures 5(a) and (b) correspond to DQWs (A) and (B), respectively. Solid and dashed curves are plotted for $\tau_p = 1.76$ ps (zero-phase shift) and for $\tau_p = 2.2$ ps (π-phase shift). The upper and lower panels correspond to $\Delta\omega = 0$ and $\Omega_T/2$.

dephasing relaxation. This process is slower than the intersubband relaxation, e.g., $\tau_0 > \tau_1$ (see numerical values above). For this reason the oscillations last for a longer time. Figures 4 and 5 show these features of the dipole moment in the cases of zero-phase shift ($\Omega_T\tau_p = 4\pi$) and π-phase shift ($\Omega_T\tau_p = 5\pi$) as indicated in figure captions. Figure 4 has been calculated for $\eta = 0$, when the two tunnel-coupled states resonate, and it corresponds to applied electric fields of 7 kV cm^{-1} (DQW (A)) and 2 kV cm^{-1} (DQW (B)), respectively. Figure 5 has been calculated for $\eta = 0.7$, out of the resonance of the tunnel-coupled levels. In this situation the electronic concentration mainly occupies the left-hand well and the oscillation amplitude becomes quenched.

The influence of the detuning frequency when $\eta = 0$ can be explained as follows. If $\Delta\omega = 0$ (upper panel of figure 4), a fast transfer of the electron density from the well in which electrons were initially created to the other well occurs. For $\Delta\omega = \Omega_T/2$ (lower panel of figure 4), the electron density oscillates between coupled levels from the beginning of the excitation. Out of the resonance between the tunnel-coupled levels ($\eta \neq 0$, figure 4) most of the electron density remains in the left-hand well and the transfer does not become effective because of level decoupling. The practical disappearance of the oscillations when $\Delta\omega = \Omega_T/2$ is especially striking.

4. Nonlinear coherent response

Now we turn to the description of the nonlinear response. In order to do this we will take into account the Coulomb renormalization of the level splitting energy, when $\mathbf{n}_t$ is governed by the nonlinear system of equation (7), and $\mathbf{L}_t$ is determined through equation (12). The characteristic concentration, $\mathcal{N}$, directly related to the pulse excitation density, is responsible for the nonlinearity. In order to get an effective Coulomb renormalization we have used $\mathcal{N} \gtrsim 2 \times 10^{10}$ cm^{-2} (corresponding to an excitation energy density of about 0.2 μJ cm^{-2}) when the nonlinear response becomes noticeable.

Figures 6(a), (b) show the evolution of the dipole moment, n_t^z, corresponding to a characteristic concentration of $\mathcal{N} \sim 0.14 n_{2D}(\tau_p\Omega_T/\pi)^2$, at the coupled-level resonance

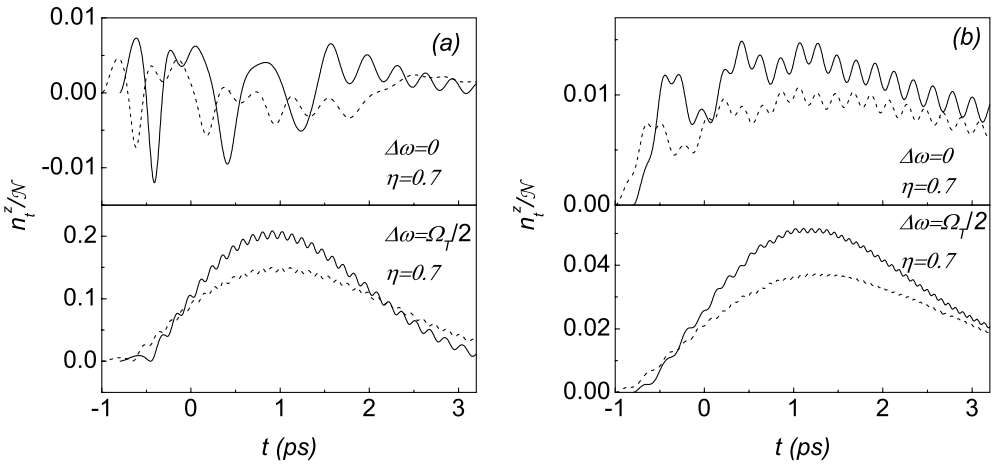

Figure 7. The same as in figure 6 for $\eta = 0.7$.

($\eta = 0$), zero-phase shift, and for structures (A) and (B), respectively. We should always keep in mind that $\mathcal{N}$ depends on τ_p^2. Thus, for a fixed excitation energy, we have a different $\mathcal{N}$ value for each pulse duration. The main result we can observe is that the oscillation period decreases and this is caused by a high $\mathcal{N}$ value. This period also depends on the detuning frequency. As a consequence of this dependency, a slight Coulomb-induced variation appears between different τ_p and $\Delta\omega$ cases. This behaviour is more noticeable in structure (B) than in (A) because the relation $\mathcal{N}\pi e^2 Z/\epsilon T$, which mainly determines the Coulomb effects in equation (7) (see [12]), is greater in the former case for the same characteristic concentration because of the different values of $v_\perp$. Another feature induced by the Coulomb interaction occurs while the excitation pulse is acting on the samples. The term $\Delta\omega+\Omega_T/2$, which initially controls n_t (and dipole moment oscillations), loses part of its importance and the masking of the intersubband oscillations diminishes.

By comparing figures 6 with 4 one can see a slight displacement of the electronic concentration to the left-hand QW caused by the above-mentioned Coulomb renormalization when $\Delta\omega = 0$ (upper panels). Once again the detuning frequency plays the main role in the oscillatory behaviour, leading to a carrier concentration, which is located in the left-hand well, one order of magnitude higher for $\Delta\omega = \Omega_T/2$ than for $\Delta\omega = 0$. Such a behaviour is common for both samples studied.

We have already shown (figure 5) that, being out of the resonance condition (e.g. $\eta = 0.7$), differences produced by the detuning frequency are small, and this kind of behaviour remains when the Coulomb renormalization is introduced (figures 7(a), (b)). However, there is a clear dissimilarity between structures (A) and (B). In the first sample the electronic concentration oscillates between the two wells from when the excitation pulse is switched on (figure 7(a)). Such behaviour is caused by a new situation of resonance at $\eta \neq 0$. To understand this point we must underline that the η-values corresponding to resonance and off-resonance are strictly defined for the linear response. When the level renormalization is included resonance conditions vary and, hence, the electric fields to get them will also vary. In the other case, and for the same reason, electrons always prefer to stay mainly in the left-hand QW (figure 7(b)). These different behaviours are caused by the opposite sign in the expression for the Coulomb level splitting renormalization (equation (12)). Finally, one can observe as a general behaviour that the dipole moment oscillations are weak in structure (A). Furthermore, for both structures,

the temporal evolution of the dipole moment loses its oscillatory behaviour almost completely when $\Delta\omega = \Omega_T/2$, the evolution depending essentially on the total concentration of excited electrons.

5. Concluding remarks

Summarizing, we have described the coherent dynamics of electrons in DQWs by taking into account the peculiarities of the intersubband excitation and relaxation for transitions between single and tunnel-coupled states. The temporal dependences of the photoinduced carrier concentration and the dipole moment are obtained both for the second-order response and the nonlinear regime, when the splitting energy is renormalized by the photoexcited charge.

Furthermore, we discuss the assumptions made. Excluding the intersubband polarization at the mid-IR frequency, we only consider pulse durations longer than the period of excitation and the short-pulse approximation in section 3 is restricted by this assumption. Both the tight-binding approximation for the description of the tunnel-coupled states and the use of the parabolic dispersion laws are valid for the DQWs under consideration with an accuracy of 10% or better. The overlap between the single-level and the lower tunnel-coupled state is neglected in the calculation of the intersubband velocity matrix element because it is a small contribution to the generation rate. The simple relaxation time approach is also widely used for the description of similar structures. The above-used dephasing and population relaxation times were taken from the experimental data for similar structures [15–17]. In applying the single-particle description of the high-frequency response we have neglected the Coulomb renormalization of the intersubband transitions due to depolarization and exchange effects, so that the nonlinear regime of the response under a not very low pump intensity may take place if Δ is not very big. On the other hand, we do not consider here the high-intensity pump case, restricting ourselves to the inequality $\mathcal{N} < n_{2D}$ when there are not Rabi oscillations (see the consideration in [18]). In addition, a self-consistent description of levels leads to a weak modifications of response. All these conditions are satisfied for the concentrations and intensities used in sections 3 and 4.

To conclude, the peculiarities of coherent dynamics under the intersubband transitions of electrons described in sections 3 and 4 are interesting in order to select effective conditions both for the THz emission, observed only under the interband excitation, and for the redistribution of the photoinduced carrier concentration (see recent mid-IR measurements in a single QW [3]). In addition, an investigation of tunnel-coupled structures is interesting for intersubband devices such are quantum cascade lasers or quantum well infrared photodetectors. It would also be interesting to verify scattering mechanisms by the use of this approach and to study the high-intensity pump, when an interplay between the nonlinear dynamics and Rabi oscillations appears. This case requires a special consideration.

Acknowledgments

This work has been supported in part by Consejería de Educación, Cultura y Deportes, Gobierno Autónomo de Canarias and by Science Foundation Ireland.

References

[1] Rossi F and Kuhn T 2002 *Rev. Mod. Phys.* **74** 895
[2] Elsaesser T and Woerner M 1999 *Phys. Rep.* **321** 254

[3] Woerner M, Kaindl R A, Eickemeyer F, Reimann K, Elsaesser T, Weiner A M, Hey R and Ploog K H 2002 *Physica* B **314** 244
[4] Waldmuller I S, Woermer M, Forster J and Knorr A 2003 *Phys. Status Solidi* **238** 474
[5] Allen L and Eberly J H 1987 *Optical Resonance and Two-Level Atoms* (New York: Dover)
Scully M O and Zubairy M S 1997 *Quantum Optics* (Cambridge: Cambridge University Press)
[6] Tamborenea P and Metiu H 1998 *Phys. Lett.* A **240** 265
Rufenacht M, Tsujino S, Allen S J, Schoendeld W and Petroff P 2000 *Phys. Status Solidi* b **221** 407
Tsujino S, Rufenacht M, Miranda P, Allen S J, Tamborenea P, Schoendeld W, Herold G, Lupke G, Lundstrom T, Petroff P, Metiu H and Moses D 2000 *Phys. Status Solidi* b **221** 391
[7] Julien F H, Gauthier-Lafaye O, Boucaud Ph, Sauvage S, Lourtioz J-M, Thierry-Mieg V and Planel R 1998 *Intersubband Transitions in Quantum Wells* ed S S Li and Y-K Su (Boston, MA: Kluwer–Academic)
Gauthier-Lafaye O, Sauvage S, Boucaud P, Julien F H, Prazeres R, Glotin F, Ortega J-M, Thierry-Mieg V, Planel R, Leburton J-P and Berger V 1997 *Appl. Phys. Lett.* **70** 3197
[8] Vasko F T and Raichev O E 1995 *Phys. Rev.* B **51** 16965
[9] Vasko F T and Kuznetsov A 1998 *Electronic States and Optical Transitions in Semiconductor Heterostructures* (New York: Springer)
[10] Gmachl C, Capasso F, Sivco D L and Cho A Y 2001 *Rep. Prog. Phys.* **64** 1533
[11] Vasko F T and Raichev O E 1995 *JETP* **81** 1146
[12] Raichev O E 1995 *Phys. Rev.* B **51** 17713
Raichev O E, Vasko F T, Hernández-Cabrera A and Aceituno P 1997 *Phys. Rev.* B **56** 4802
[13] Vasko F T 2001 *JETP* **93** 1279
[14] See, for example, Nag B R 2000 *Physics of Quantum Well Devices* (Dordrecht: Kluwer–Academic)
Ferry D K and Grondin R O 1991 *Physics of Submicron Devices* (New York: Plenum)
[15] Sekine N, Hirakawa K and Arakawa Y 1998 *Japan. J. Appl. Phys.* **37** 1643
Wolter F, Roskos H G, Bolivar P H, Bartels G, Kurz H, Köhler K, Grahn H T and Hey R 1997 *Phys. Status Solidi* b **204** 83
[16] Lavon Y, Sa'ar A, Julien F, Leburton J-P and Planel R 1998 *Intersubband Transitions in Quantum Wells* ed S S Li and Y-K Su (Boston, MA: Kluwer–Academic)
[17] Unuma T K, Takahashi T, Noda T and Yoshita M 2001 *Appl. Phys. Lett.* **78** 3448
[18] Vasko F T, Hernández-Cabrera A and Aceituno P 2004 *Semicond. Sci. Technol.* **19** S179